Extracting reliable electronic properties from transmission spectra of indium tin oxide thin films and nanocrystal films by careful application of the Drude theory

Rueben J. Mendelsberg, Guillermo Garcia, and Delia J. Milliron

Citation: J. Appl. Phys. **111**, 063515 (2012); doi: 10.1063/1.3695996
View online: http://dx.doi.org/10.1063/1.3695996
View Table of Contents: http://jap.aip.org/resource/1/JAPIAU/v111/i6
Published by the American Institute of Physics.

Extracting reliable electronic properties from transmission spectra of indium tin oxide thin films and nanocrystal films by careful application of the Drude theory

Rueben J. Mendelsberg,[1,2] Guillermo Garcia,[2] and Delia J. Milliron[2,a)]
[1]*Lawrence Berkeley National Laboratory, Plasma Applications Group, Berkeley, California 94720, USA*
[2]*Lawrence Berkeley National Laboratory, The Molecular Foundry, Berkeley, California 94720, USA*

(Received 8 October 2011; accepted 20 February 2012; published online 23 March 2012)

Analysis of the transmittance and reflectance of transparent conducting oxide thin films and nanocrystal films can be accurately modeled using the Drude free electron theory to extract electrical transport properties if enough care is taken. However, several fits starting from different initial guesses are needed before confidence in the extracted Drude parameters can be obtained. Film thickness, optical carrier concentration, and optical carrier mobility can be reliably derived when using either a fully empirical or semiempirical model for the ionized impurity scattering. The results are in good agreement with those based on more arduous spectroscopic ellipsometry measurements. Furthermore, fitting the reflectance along with the transmittance reduces the uncertainty, but does not significantly affect the values of the extracted parameters. © *2012 American Institute of Physics*. [http://dx.doi.org/10.1063/1.3695996]

I. INTRODUCTION

Shortly after J. J. Thomson discovered the electron,[1] Paul Drude formulated his theory,[2] based on the idea that essentially free electrons are responsible for the electrical conduction in metals. While his classical treatment failed at describing the specific heat of metals, it has proven surprisingly effective at connecting electronic and optical properties of conductive materials. As such, the Drude theory has been used extensively for many decades to derive essential electronic characteristics from the observed optical properties of metals,[3,4] semiconductors,[5] several conductive oxides,[6–12] and, recently, graphene.[13]

High performance transparent conductive oxides (TCOs)—used in flat panel displays, solar cells, and dynamic window coatings—are degenerately doped wide-gap semiconductors with significant free electron concentrations (10^{19}–10^{21} cm^{-3}). These electrons originate from ionized impurities, which also act as scattering centers. The Drude theory must be modified to account for impurity scattering when interpreting optical measurements of TCOs. There are a few published models which account for the ionized impurity scattering in TCOs,[9,14,15] but a systematic comparison has yet to be published.

Spectroscopic ellipsometry (SE) provides perhaps the richest optical data for Drude analysis of thin films. However, SE requires specialized equipment and is not universally available, motivating the development of reliable methods for Drude analysis of transmittance (T) and/or reflectance (R) data. The advantage is that T and R measurements can be performed quickly using common equipment in a simple geometry. Extraction of the optical constants as a function of wavelength using T and R by iterative computational methods was first demonstrated by Bennett and Booty in 1966.[16] Since that work and the remarkable advance of the personal computer, analysis of T and R spectra using the Drude theory has become routine for thin films. A new wave of interest in Drude analysis has accompanied the surge of research on plasmonic nanomaterials. However, care is required to extract meaningful electronic properties, especially for nanostructured systems.

In this work, we present a systematic comparison of two different models, which account for ionized impurity scattering within the framework of the Drude theory. We show that both models are successful at describing the observed T and R of indium tin oxide (ITO) thin films. Embedding the modified Drude theory within an effective medium approximation, we also succeed in relating T and R spectra of ITO nanocrystal films to electronic properties.

For both thin films and nanocrystal films, good agreement was observed with parameters obtained from SE. Furthermore, we show that meaningful results can be obtained when only T measurements are available. While the focus of this work is on TCOs, the methodology described here may also be applicable to other degenerately doped semiconductors.

II. EXPERIMENTAL

The ITO nanocrystals used in this study were prepared by organic-phase colloidal synthesis, as described in earlier work.[17] After synthesis, surface-bound oleic acid ligands facilitate effective dispersion of the ITO nanocrystals in non-polar solvents. Optical quality films of ITO nanocrystals were prepared by spin-coating on quartz substrates followed by an *in situ* ligand exchange and subsequent annealing at 250 °C in Ar. Film preparation is described in detail in Ref. 17. To establish our optical model and for comparison, a commercially available ITO thin film (Thin Film Devices) with a sheet resistance of 20 Ω was also studied.

a)Electronic mail: dmilliron@lbl.gov.

For this work, the ITO nanocrystals were about 4.5 nm in diameter and had a Sn content of about 14 at.%, as measured by inductively coupled plasma optical emission spectroscopy. The fully processed nanocrystal film was 190 ± 10 nm thick (measured by stylus) and had a dc sheet resistance around 4.5 MΩ. A scanning electron microscope (SEM) image of this nanocrystal film is shown in Fig. 1(a) and indicates a porous network. Transmission electron microscopy of one of these nanocrystals is shown in the inset of Fig. 1(a). Figure 1(b) shows a film prepared the same way with larger nanocrystals (8 nm in diameter), where the interconnected nanocrystal network can be easily resolved by SEM. X ray diffraction (XRD) from the 4.5-nm nanocrystal film, shown in Fig. 1(c), gave the characteristic peaks of cubic indium oxide. From a pseudo-Voigt decomposition of the (222) and (400) peaks, a grain size of about 4.5 nm can be extracted using the Scherrer equation after correcting for machine broadening, which agrees well with the nanocrystal diameter.

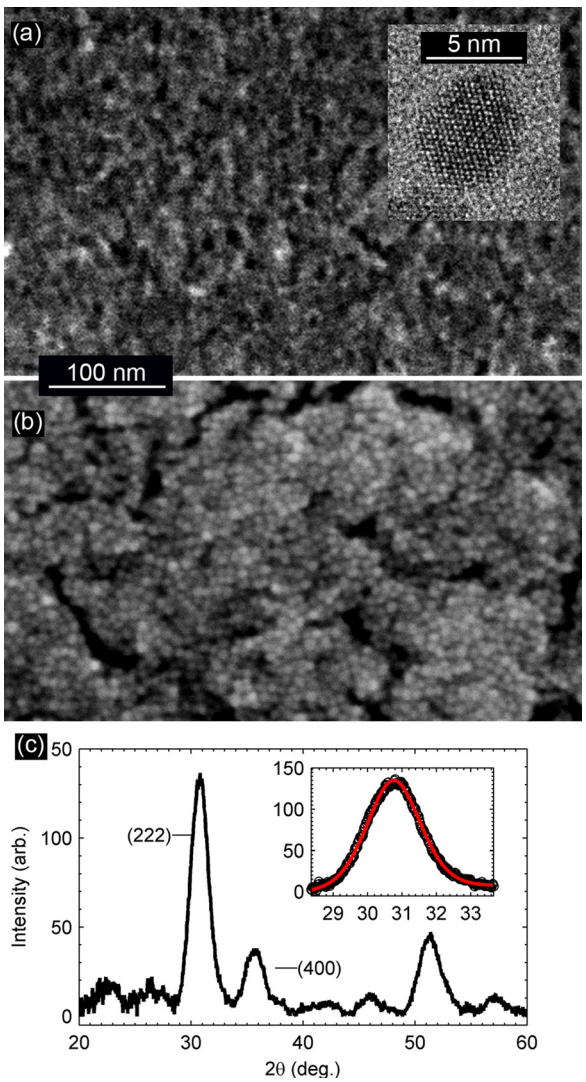

FIG. 1. Scanning electron micrographs of ITO nanocrystal films. The top image (a) shows the nanocrystal film used in this work along with a high resolution transmission electron microscope image of a single nanocrystal. A nanocrystal film made under similar conditions with larger nanocrystals is shown in (b) in order to easily see the packing. An XRD pattern of the smaller nanocrystals is shown in (c) with the pseudo-Voigt decomposition of the (222) peak shown in the inset.

Transmittance (T) and specular reflectance (R) were measured over the 190–2500 nm range using a Perkin-Elmer Lambda 950 spectrophotometer equipped with a universal reflectance attachment. T measurements were taken at normal incidence, while R was taken near-normal at 8°. For comparison, SE measurements were recorded using a Horiba Jobin Yvon UVISEL over the 190–2175 nm range. Hall measurements of the commercial ITO thin film were made at room temperature using an Ecopia HMS3000 Hall effect measurement system equipped with a 0.6 T magnet.

Modeling of the dielectric function from all the T, R, and SE measurements was carried out using the Scout software package (www.wtheiss.com) by employing several built-in optical models, including the extended Drude theory, which is the focus of this report. An initial guess to the parameters of the optical model must first be provided by the user. Scout then uses the downhill simplex method to adjust the parameters in order to minimize the mean-square-error between the measured and calculated T, R, and SE data. The minimization process iterates until the mean-square-error converges to within a small tolerance.

It was observed that there may be several local minima in the mean-square-error function, leading to more than one physically reasonable combination of parameter values, which describe the measured data well. To account for this and to get enough statistics, the fitting procedure was repeated 10 times for each spectrum, each time using a different initial guess. Care was taken to ensure each initial guess was sufficiently different from the others. For example, after the first fit, a general idea of the best-fit parameters was obtained. Subsequent fits to the same spectra were thus started from both above and below these values in several different permutations. For the rest of this work, a "fit" is defined as a particular combination of parameter values, which reproduces the measured data (10 fits for every spectrum). A few initial guesses with extreme values for several parameters were also explored for each spectrum. This semi-random method proved to quickly and easily explore a large region of parameter space.

For some of the fits, one or more of the parameters' ranges were bounded, with the fit results occasionally running up against the limits. This was mainly done to keep parameters within physically reasonable values. Also, bounding the parameters prevented the algorithm from always converging to the same fit with the smallest mean-square-error when other fits with acceptably larger error also provided physically reasonable parameter values. Furthermore, performing several fits with bounded parameters allowed for observation of parameter correlations, which must be explored to gain confidence in all the extracted free parameter values.

III. OPTICAL MODEL

To successfully fit the T and R spectra, an accurate model for the electronic susceptibility (χ) must be constructed. Here, we use a four-part, frequency (ω)-dependent model given by

$$\chi(\omega) = \epsilon_B + \chi_{BG}(\omega) + \chi_{UV}(\omega) + \chi_D(\omega), \quad (1)$$

where the first part, ϵ_B, is a constant representing the dielectric background. Some authors refer to ϵ_B as the high frequency dielectric constant ϵ_∞. However, the other components of χ can potentially influence the high frequency optical response.

χ_D, containing the electronic parameters of interest, is the contribution from the free carriers (here electrons) as described by the Drude theory. The Drude susceptibility is given by

$$\chi_D(\omega) = -\frac{\omega_P^2}{\omega^2 + i\omega\Gamma(\omega)}, \quad (2)$$

where ω_P is the plasma frequency and $\Gamma(\omega)$ is the frequency-dependent damping constant. The plasma frequency is related to the free-carrier concentration by $\omega_P^2 = ne^2/m^*\epsilon_0$, where n is the carrier concentration, e is the elementary charge, m^* is the electron effective mass, and ϵ_0 is the permittivity of free space.

The frequency dependence of the damping constant can be described using a purely empirical formula,

$$\Gamma(\omega) = \Gamma_L - \frac{\Gamma_L - \Gamma_H}{\pi}\left[\arctan\left(\frac{\omega - \Gamma_X}{\Gamma_W}\right) + \frac{\pi}{2}\right], \quad (3)$$

where Γ_L is the low frequency damping constant, Γ_H is the high frequency damping constant, Γ_X is the cross-over frequency, and Γ_W is the cross-over width. Alternatively, a semiempirical model may be used that accounts for the fact that ionized impurity scattering is the dominant carrier scattering mechanism in TCOs at optical frequencies.[14] Based on energy loss calculations by Gerlach,[18] the following can be used in place of Eq. (3):[9]

$$\Gamma(\omega) = f(\omega)\Gamma_L + (1 - f(\omega))\Gamma_H\left(\frac{\omega}{\Gamma_X}\right)^{-3/2}, \quad (4)$$

where

$$f(\omega) = \frac{1}{1 + \exp\left(\frac{\omega - \Gamma_X}{\Gamma_W}\right)}. \quad (5)$$

This model is essentially the same as that used by Ederth *et al.* to model the transmittance of ITO films,[19] except for the introduction of the crossover function (Eq. (5)), which provides a smooth transition from the low to high frequency ranges.

The damping constant, $\Gamma(\omega)$, is the inverse relaxation time of the electrons, and its low frequency limit is related to the optically derived dc electrical mobility (μ_{opt}). Using the empirical model (Eq. (3)), μ_{opt} is given by $\mu_{opt} = e/m^*\Gamma(0)$, and for the semiempirical model (Eq. (4)), it is $\mu_{opt} = e/m^*\Gamma_L$.

While these Drude parameters are of primary interest, the other components to $\chi(\omega)$ shown in Eq. (1) need to be addressed with some care, as they can impact the quality and interpretation of the fitting results across the ultraviolet (UV) to near infrared (NIR) range. The band-gap absorption ($\chi_{BG}(\omega)$) was described by the O'Leary-Johnson-Lim (OJL) model.[20] This model was originally designed for amorphous semiconductors. It assumes a completely filled parabolic valence band and an unfilled parabolic conduction band. It also assumes an exponentially decaying density of states within the band-gap for both the valence and conduction bands. Qualitatively, it does an adequate job modeling the band-gap absorption for degenerately doped TCOs, as demonstrated by several authors for ITO.[15,21,22] However, the assumption of a parabolic conduction band (away from the exponential tail states) is not quantitatively justified.[6,9] Furthermore, many-body effects distort the band structure for semiconductors with high electron concentrations.[23] Thus, we do not place much confidence in the band-gap parameters extracted from the OJL model, but do find it adequate to fit the band-gap absorption without unduly perturbing the Drude fitting.

The third term in the susceptibility, χ_{UV}, represents UV absorption deep into the conduction band and has been used in the past for modeling T and R in ITO.[15] Without this empirical term, the fits are very poor and result in unreasonable values for most of the other parameters in χ. For this work, χ_{UV} was modeled as a simple harmonic oscillator. For all the fits in this work, the frequency of this harmonic oscillator (ω_{UV}) was not crucial to the fit quality or the values of the other parameters and ω_{UV} was typically restricted to above 60 000 cm^{-1} (7.4 eV). The need for χ_{UV} in the optical model may be due to the inaccuracy of the OJL model for a partially filled, non-parabolic conduction band.

Once the model for $\chi(\omega)$ has been chosen, a layer stack needs to be defined. For the ITO commercial thin film, the stack consisted of 1 mm of glass supporting a thin film of ITO. For the nanocrystal film, an effective medium approximation was used to describe the thin film layer, as discussed later in detail. No additional roughness layer was needed to obtain very nice fits in both cases.

The best fits to the T and R data were obtained when using the *absolute* spectra. Thus, no blank substrate was put into the reference beam path of the spectrophotometer when taking T measurements. R measurements were taken in absolute reflectance mode, a feature of the universal reflectance attachment which removes the requirement for a reference mirror. However, when using absolute T and R spectra, the optical constants of the substrate need to be known to high accuracy. Thus, one of the commercial ITO thin films from the same batch was etched off the glass substrate by soaking in concentrated HCl solution overnight. T and R of the substrates were collected and fit using many free parameters in order to accurately describe the *shape* of the substrate dielectric function. All these parameters were fixed when fitting the ITO/glass stacks. Accurate fitting of the substrate is paramount to successful fits of the film stacks, and relying on an external database of optical constants is not recommended.

IV. RESULTS AND DISCUSSION

A. Commercial ITO thin film

We optimized and validated our fitting procedure using a commercially available ITO thin film on glass. Both models for $\Gamma(\omega)$ were successful at modeling T and R spectra.

Figure 2 shows the measured data along with one example of the fit (using Eq. (3)). Tables I and II summarize the parameters found with the two damping models for the ten different fits of R and T (simultaneously). Here, the "min" and "max" values represent the extreme values of each of the parameters individually. Half the difference between the "min" and "max" is a good estimate of the uncertainty in the fit parameters. Equations (3) and (4) provided essentially the same quality of fit, as indicated by the mean-square-error (δ).

The first conclusion to be drawn from the data is that one fit per spectrum is certainly not enough to establish confidence in the values of all the free parameters in the model. Several fits need to be carried out for each sample to assess the reliability of their converged values. In other words, several different parameter combinations gave roughly the same δ. The overall best fits are shown in all the figures in this work, but essentially no difference could be observed by eye between all the fits for a measured spectrum.

The second lesson is that the thickness (d) showed very little variation over all the fits using both models for $\Gamma(\omega)$. As such, this fitting technique is ideal for optical thickness measurements when interference fringes are clearly visible in the spectra. The film thickness was in excellent agreement with the 140 ± 5 nm measured by profilometry. It may be tempting to use the thickness agreement as an indicator of confidence in all parameters' values, as has been argued in some published work. However, this should rather be taken as an indication that many fits using drastically different initial guesses and varying parameter limits need to be carried out to clearly identify the uncertainty in each of the parameter values ultimately determined.

The plasma frequency (ω_P) also showed very little variation and agreed well between the two models for $\Gamma(\omega)$. Optical-derived carrier concentration (n_{opt}) was calculated from all 20 fits to be $(8.2 \pm 0.5) \times 10^{20}\,\mathrm{cm}^{-3}$ using an effective electron mass of $0.4\,m_e$.[7,9] Hall measurements, taken on the same sample the same day as the optical measurements, gave a Hall carrier concentration of $n_H = (8.0 \pm 0.07) \times 10^{20}\,\mathrm{cm}^{-3}$.

Optical mobility (μ_{opt}) was also determined from this data, but a larger spread in the values was observed when comparing fits to Eqs. (3) and (4). When using Eq. (3), a value of $\mu_{opt} = 24 \pm 1\ \mathrm{cm}^2/\mathrm{Vs}$ was obtained from the 10 fits, with very little uncertainty. On the other hand, a large spread in μ_{opt} was obtained when using Eq. (4) with $\mu_{opt} = 25 \pm 13\ \mathrm{cm}^2/\mathrm{Vs}$ after ignoring 2 unphysical values of $\Gamma_L = 0\ \mathrm{cm}^{-1}$. Hall measurements give a mobility of $\mu_H = 30 \pm 2\ \mathrm{cm}^2/\mathrm{Vs}$. Like n_H, μ_H is higher than the optical value, which may also be due to the non-parabolicity of the conduction band.

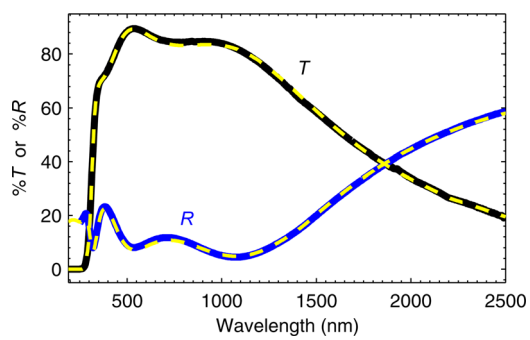

FIG. 2. Absolute reflectance (R) and transmittance (T) of commercially available ITO on glass. Fits to the data are shown as the dashed (yellow) lines.

TABLE I. Comparison of the Drude parameters extracted using Eq. (3) or Eq. (4) when fitting T and R (simultaneously) of a commercial ITO thin film. Ten fits using each model were performed on the spectra shown in Fig. 2. The unit for δ is $\%T$ (or $\%R$), film thickness (d) is in nm, and the Drude parameters are in cm^{-1}.

Model		δ	d	ω_P	Γ_L	Γ_H	Γ_X	Γ_W
Eq. (3)	Min	0.00320	142	13 353	940	248	6000	500
	Max	0.03492	148	13 985	1141	600	10 415	6000
	Mean	0.01391	145	13 623	1000	503	8997	2126
Eq. (4)	Min	0.00246	144	13 313	0	0	4200	828
	Max	0.01998	148	13 831	2010	1889	13 487	10000
	Mean	0.00684	146	13 500	821	822	8779	2536

The agreement between the values of μ_{opt} obtained with Eqs. (3) and (4) lends confidence to the validity of Eq. (3). Furthermore, the minimal uncertainty obtained with the fully empirical Eq. (3) indicates a more stable fitting process compared to the semiempirical Eq. (4). This is further confirmed by the smaller uncertainty in all of the converged parameter values shown in Tables I and II.

While the individual parameters show less variation when using Eq. (3), the overall damping function, $\Gamma(\omega)$, converges more reliably using Eq. (4) (Fig. 3). However, this simply underscores the instability in the Drude damping parameters extracted using Eq. (4), since a large spread in their values gives nearly the same $\Gamma(\omega)$.

Figure 4 shows the refractive index, n and k, calculated for all the fits using $n + ik = \sqrt{\epsilon_1 + i\epsilon_2}$. These curves match well with previous reports for ITO,[6–8,24] and there is excellent agreement for all fits and between both models, except for the band-gap region. As discussed previously, the OJL model is not ideal for ITO, and Table I shows the average band-gap was found to be higher for Eq. (4).

Considering the confidence in fitting parameters for the two alternative damping functions and the agreement with Hall measurements, Eq. (3) was used for $\Gamma(\omega)$ in the rest of this work. The increased stability of the fit parameters and the realistic n and k values achieved with Eq. (3) outweigh the conceptual benefits of using the semiempirical Eq. (4)

TABLE II. Comparison of the OJL parameters, UV harmonic oscillator parameters, and dielectric background when using Eq. (3) or Eq. (4) when fitting T and R of a commercial ITO thin film. Ten fits using each model were performed on the spectra shown in Fig. 2.

Model		E_g (eV)	γ_{OJL} (eV)	S_{OJL}	D_{OJL}	ω_{UV} (cm^{-1})	S_{UV}	Γ_{UV} (cm^{-1})	ϵ_B
Eq. (3)	Min	3.50	0.038	1.05	15 583	60 000	500	0	2.09
	Max	3.84	0.16	2.31	23 479	85 000	53 996	30 412	3.75
	Mean	3.66	0.12	1.52	18 937	76 266	18 196	16 260	2.92
Eq. (4)	Min	3.52	0.080	0.95	2862	45 000	1650	1042	0.88
	Max	4.50	0.25	15.0	45 120	100 000	50 000	60 000	3.70
	Mean	3.94	0.17	5.50	19 099	67 678	18 226	19 427	2.54

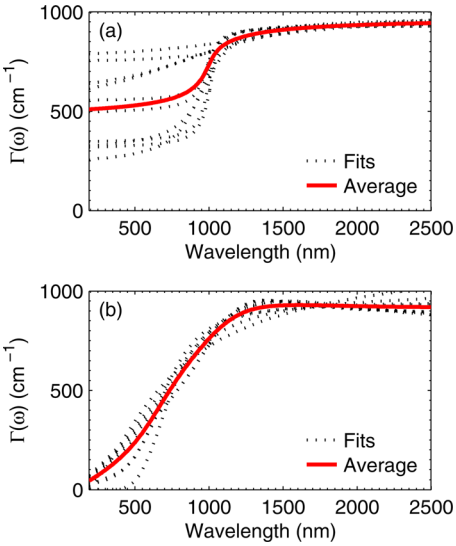

FIG. 3. Damping constant calculated from the fits of (a) Eq. (3) and (b) Eq. (4). The dotted (black) lines show each fit and the solid (red) lines show the average.

when n_{opt} and μ_{opt} are the parameters of interest. Also, the fitting algorithm converged more quickly using Eq. (3). However, a physically meaningful analysis of the scattering mechanisms in a TCO sample and their relationship to $\Gamma(\omega)$ would require a more detailed and rigorous treatment.

B. Nanocrystal thin films

Our systematic analysis and optimization of the fitting procedure for the commercial ITO thin film forms a sound basis for extracting meaningful electronic properties from the T and R spectra of ITO nanocrystal films. Here, we need to account for the host matrix surrounding the nanocrystals as well as the crystals themselves. Since the granularity of nanocrystal films is on a length scale smaller than the wavelength of the light, an effective medium approximation (EMA) can be used. The Bruggeman approximation[25] is the most commonly used EMA for nanocrystal films.[12,19] It accounts for electrical conduction between nanocrystals when the volume fraction (f_V) of the nanocrystals in the film is above a percolation threshold of 0.33. However, this EMA did not fit the data well, which was initially surprising, since Fig. 1 shows that the nanocrystals are in physical contact with several nearest neighbors, indicating a relatively high f_V for the ITO nanocrystal films.

Good fits to the T and R spectra of the ITO nanocrystal film were obtained when using the relatively simple Maxwell-Garnett[26] (MG) EMA, as shown in Fig. 5. The MG approximation only assumes spherical particles with a dipole polarizability and does not account for conduction between nanocrystals. It is typically used when the volume fraction of the crystals is small. The MG approximation also ignores any dipole coupling between the nanocrystals, which is known to shift the surface plasmon resonance energy for plasmonic "molecules" consisting of metallic nanocrystals in close proximity.[27] However, less is known in regarding plasmon coupling among a large ensemble of oxide nanocrystals.

The fit parameters extracted using the MG approximation are listed in Table III. Again, very little variation in the film thickness and ω_P was observed for the 10 fits, but the fits did slightly underestimate the 190 ± 10 nm measured by profilometry. Carrier concentration of these nanoparticles calculated from ω_P was $n_{opt} = (1.07 \pm 0.05) \times 10^{21}$ cm^{-3}, higher than the ITO thin film and showing that only about 10% of the Sn contributes to the room temperature conductivity. Optical mobility showed a larger variation and was $\mu_{opt} = 8.5 \pm 1.1$ cm^2/Vs. The relatively low μ_{opt} compared to the commercial thin film can be ascribed to an additional scattering mechanism arising from the surface of the nanocrystals. Resistivity inside the nanocrystals calculated from this optical data was $\rho_{opt} = 1/n_{opt} e \mu_{opt} = (7 \pm 1) \times 10^{-4}$ Ωcm, about twice that of the commercial thin film ($\rho_{opt} = (3.2 \pm 0.4) \times 10^{-4}$ Ωcm).

The low value of ρ_{opt} compared to the ≈85 Ωcm measured by a 4-point probe suggests an explanation for why the MG effective medium approximation fits the data while the Bruggeman approximation does not. The high volume fractions, f_V, shown in Fig. 6 clearly indicate the nanocrystals

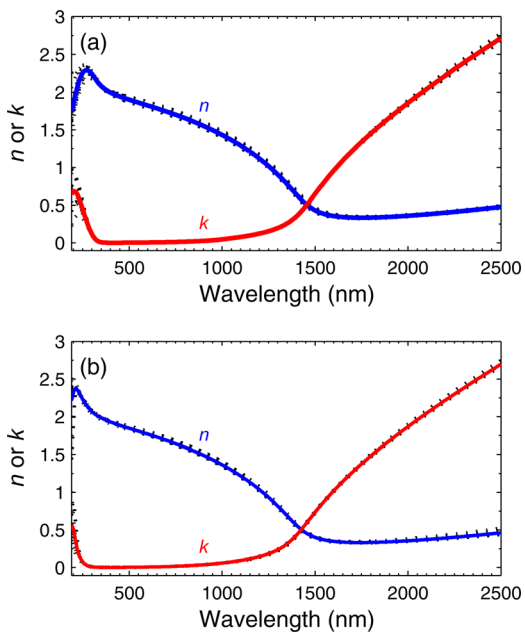

FIG. 4. n and k calculated from the dielectric function when using (a) Eq. (3) and (b) Eq. (4) to fit T and R. The dotted (black) lines show each fit and the solid (red and blue) lines show the average.

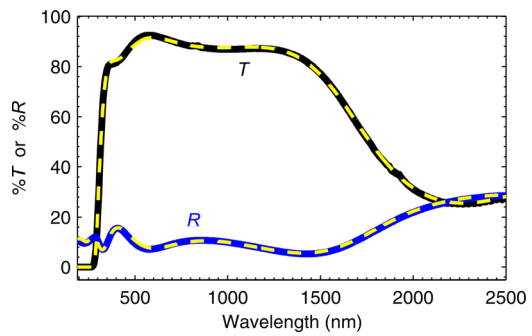

FIG. 5. Measured T and R (solid lines) and fits (dashed yellow lines) of a nanocrystal ITO film. The Maxwell-Garnett effective medium approximation was used along with Eq. (3).

TABLE III. Drude parameters extracted using Eq. (3) and the MG effective medium approximation when fitting T and R of a nanocrystal film. Ten fits were performed on the spectra shown in Fig. 5. The units are the same as those in Table I.

	δ	d	ω_P	Γ_L	Γ_H	Γ_X	Γ_W
Min	0.00530	175	15 130	2775	0	4918	1647
Max	0.01230	178	15 701	3582	0	5699	1861
Mean	0.00850	177	15 476	3058	0	5434	1701

are in physical contact, and f_V is above the percolation threshold of 0.33 used in Bruggeman's approximation. However, the particles are not well connected *electrically*, presumably because there exists substantial potential barriers between adjacent nanocrystals. This is further supported by temperature-dependent resistivity measurements discussed below. Thus, when driven by photons, the electrons are effectively stopped at the nanocrystal surface, so electrical coupling does not significantly affect the optical properties.

The sheer number of parameters required for the effective medium approximation fit causes greater uncertainty in some of the dielectric fitting results. For instance, the OJL and UV oscillator parameters shown in Table IV have a fairly large spread, and E_g is lower than expected. Nonetheless, high confidence in the value of d, n_{opt}, and μ_{opt} show the T and R analysis is useful for determining the electrical properties of the ITO nanocrystals composing the films.

However, while d of the nanocrystal film can be confidently determined, a correlation between the MG volume fraction (f_V) and host refractive index (n_{host}) can be seen in Fig. 6(a). This means that a unique, optimal solution cannot be found for the values of n_{host} and f_V. In this case, the host is known to be air, since the annealing effectively removes the ligands, as verified by IR absorbance measurements.[17] Setting $n_{host} = 1$, we find the correct volume fraction of approximately 0.6. However, if n_{host} is not known, the value of f_V needs to be determined by alternate means if an accurate value of n_{host} is desired. For example, this may be the case when analyzing nanocrystal films at different processing stages as the host (ligands) changes.

Figure 6(b) shows that a correlation also exists between the Drude parameters Γ_L and Γ_X. Fortunately, this correlation is such that Eq. (3) results in essentially the same value of μ_{opt} for all the fits. Correlation between Γ_L and Γ_X was not observed for the commercial ITO thin film, which is why the relative uncertainty of μ_{opt} was significantly less in that case. Nonetheless, this correlation shows that optimized values for Γ_L and Γ_X cannot be uniquely determined, underscoring that a detailed analysis of the carrier scattering mechanisms for nanocrystal films is not possible with the simple model for $\Gamma(\omega)$ used here.

TABLE IV. OJL and UV parameters along with the dielectric background of the particles for the ITO nanocrystal film shown in Fig. 5. Ten fits were performed on the spectra shown in Fig. 5. For the units, see Table II.

	E_g	γ_{OJL}	S_{OJL}	D_{OJL}	ω_{UV}	S_{UV}	Γ_{UV}	ϵ_B
Min	3.49	0.18	3.97	10 318	62 939	1159	1134	3.80
Max	4.00	0.33	9.02	20 496	70 000	58 979	25 000	4.70
Mean	3.82	0.26	5.88	15 301	69 257	25 977	11 028	4.26

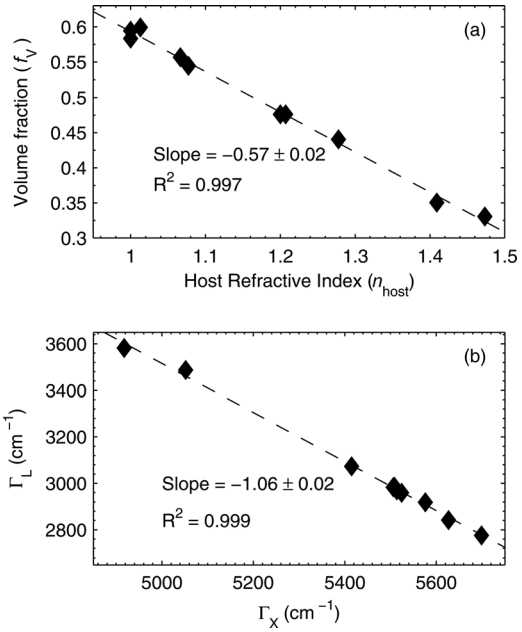

FIG. 6. Correlation of fitting parameters (a) f_V and n_{host} and (b) Γ_L and Γ_X for the nanocrystal film.

C. Deriving electronic properties from transmittance alone

For transparent samples, measuring T is quick, easy, and adaptable to a range of experimental configurations. For the best fits, both T and R should be accounted for, but several groups have neglected R in their Drude modeling. Previous studies have analyzed fits of R alone,[10,11] but the consequences of fitting T alone have not yet been systematically investigated.

The consequences on the Drude parameters of considering only T were evaluated for both the commercial thin film and nanocrystal film (Table V). In both cases, d and ω_P are quite close to those found when fitting R and T together. The damping parameters are also close, but there is a larger variation when only using T. Optical mobility calculated for the thin film and nanocrystal film was 18 ± 3 and 6 ± 3 cm^2/Vs, respectively. These values are smaller yet still in agreement with those extracted when R was accounted for. However,

TABLE V. Drude parameters extracted from the commercial thin film (TF) and the nanocrystal film (NCF) when neglecting reflectance. Ten fits were performed on only the T spectra shown in Figs. 2 and 5. The units are given in Table I.

Sample		δ	d	ω_P	Γ_L	Γ_H	Γ_X	Γ_W
TF	Min	0.00112	142	12 859	1217	0	8500	1049
	Max	0.00277	151	13 721	1872	294	10 000	5000
	Mean	0.00179	145	13 391	1426	65	9362	2072
NCF	Min	0.00162	168	14 079	2880	0	4145	1135
	Max	0.00437	174	15 852	5000	0	5579	1584
	Mean	0.00326	171	14 747	4508	0	4567	1416

the uncertainties are about 3 times larger. Also, n and k were in good agreement with those found from R and T, but again, with about 3 times the uncertainty. Thus, accurate thickness, Drude parameters, and complex refractive index can be extracted when neglecting R in the dielectric function modeling, albeit with reduced precision.

D. Comparison to ellipsometry

As discussed in the introduction, SE is perhaps the gold standard when it comes to measuring the dielectric function of thin-films. Many groups have used SE for Drude analysis of TCO's, even simultaneously fitting SE alongside R and T measurements.[28] As a final verification of the R-T and T-only methods discussed in this work, SE was performed on the thin film and nanocrystal film (Fig. 7). This data was taken at an incident angle of 70°, and the spectra were fit without accounting for T and R measurements.

The same exact layer stack and model for $\chi(\omega)$ (using Eq. (3) for $\Gamma(\omega)$) was used to fit the $I_c = \sin 2\Phi \cos\Delta$ and $I_s = \sin 2\Phi \sin\Delta$ data, as was used for the R and T analysis discussed above. Satisfactory fits to the data were obtained, but some discrepancy was observed in the near UV region, which we ascribe to the simple bandgap model. The calculated n and k values are shown in Fig. 8. The SE and R-T methods agreed to within their mutual uncertainty. For the commercial thin film, the uncertainty in n and k for the SE method was smaller than the width of the line in the plot. Clearly, SE gives smaller uncertainty, but Fig. 8 shows that R and T measurements indeed give accurate results.

Good agreement was also observed between the SE and the R-T and T-only methods for the Drude parameters, which are listed for the SE measurements in Table VI. The carrier concentrations extracted from SE for the thin film and nanocrystal film are $n_{opt} = (8.3 \pm 0.1) \times 10^{20}\,cm^{-3}$ and $n_{opt} = (9.6 \pm 0.3) \times 10^{20}\,cm^{-3}$, respectively. Optical mobility

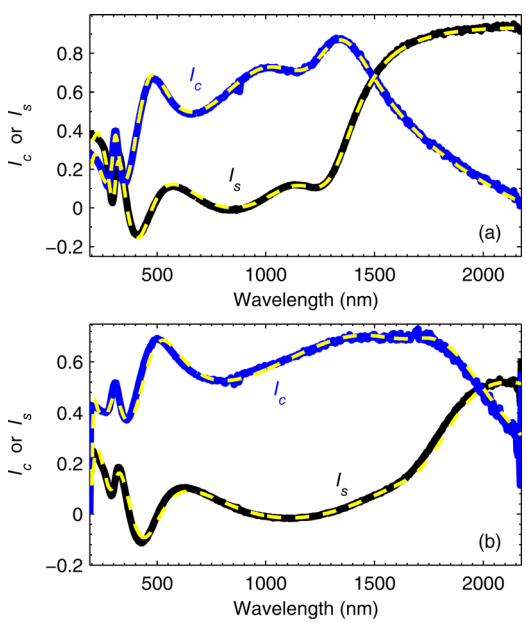

FIG. 7. Ellipsometry measurements at 70° incidence for the (a) commercial ITO thin film and (b) the ITO nanocrystal film. The (yellow) dotted lines show the fits using the same $\chi(\omega)$ as was used for the R and T fitting.

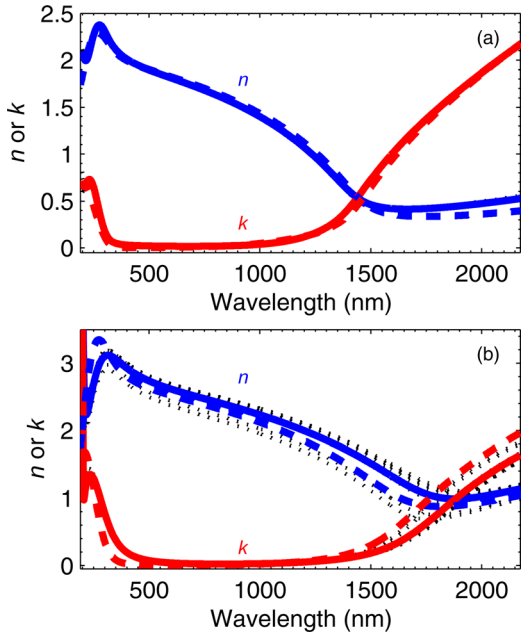

FIG. 8. Complex refractive index extracted from the ellipsometry measurements for the (a) commercial ITO thin film and (b) the ITO nanocrystal film. Ten fits were performed on the spectra; each fit is shown as a (black) dotted line, the average as the thick solid line, and the values extracted from the T and R measurements as the thick dashed lines.

was $\mu_{opt} = 16 \pm 2\ cm^2/Vs$ and $\mu_{opt} = 7.6 \pm 0.8\ cm^2/Vs$, again showing agreement with the results of the R-T and T-only methods. In fact, since our T and R measurements extend to longer wavelengths, they likely extract more physically meaningful values for the Drude parameters than our SE measurements.

Thickness was in excellent agreement for the thin film, but SE measurements show a noticeably smaller value than the R-T and T-only measurements for the nanocrystal film. A larger spread in ϵ_B, the OJL band-gap parameters, and the UV oscillator parameters was observed for the nanocrystal film compared to the thin film, as evidenced by Fig. 8. The very simple model used for the nanocrystal film may not be sophisticated enough to provide the same quality of fit to the SE as the model did for the thin film case. Nevertheless, altering the model in the nanocrystal film case by including a roughness layer or thickness gradient did not improve the fit. Furthermore, the Bruggeman effective medium approximation fit the SE data poorly. Finally, the same parameter correlations observed in Fig. 6 were also observed in the SE data.

TABLE VI. Drude parameters extracted from the commercial thin film (TF) and the nanocrystal film (NCF) by fitting the SE data. Ten fits were performed on the I_c and I_s spectra shown in Fig. 7. For the units, see Table I.

Sample		d	ω_P	Γ_L	Γ_H	Γ_X	Γ_W
TF	Min	143.0	13 622	1452	0	7655	1799
	Max	144.2	13 740	1785	0.4	8155	2895
	Mean	143.5	13 664	1548	0.1	8039	2107
NCF	Min	166.2	14 471	2910	0	4769	933
	Max	167.1	14 770	3673	313	5233	1350
	Mean	166.4	14 675	3327	139	5075	1189

It should also be noted that the commonly used Tauc-Lorentz model for the band-gap gave very similar fits to the SE and *R-T* data as the OJL model did. Better fits to the SE data for the nanocrystal film are definitely expected for a more sophisticated optical model, but the one used here was sufficient for the *R-T* and *T*-only analysis.

E. Temperature-dependent resistivity measurements

Extracting Hall data from (continuous) TCO thin films to compare with optical measurements is straight-forward and can give further insight into the conduction mechanisms.[11,29] Easy measurements can be made at room temperature in the van der Pauw geometry in low magnetic fields, due to the high carrier mobility. However, for conducting nanocrystal films with relatively high resistivity, the situation is more complicated. Hopping conduction mechanisms are typically invoked to explain measurements on nanocrystal films[30,31] and invariably lead to low Hall mobility.

Typical magnets available in common Hall measurement systems are not strong enough to produce a Hall voltage large enough for reproducible measurements on the low mobility nanocrystal samples. This is true for our system, which yields non-physical and non-reproducible results for the carrier concentration and mobility of the ITO nanocrystal film. Thus, the optical based methods are sometimes the only way to access the electrical properties of TCO nanocrystal films.

Nevertheless, the resistivity of the ITO nanocrystal film can be reliably measured in the van der Pauw geometry despite potential complications with the van der Pauw equation when voids in the sample are present. Figure 9 shows the temperature-dependent resistivity of the commercial thin film and the nanocrystal film measured in an Ecopia HMS5000 Hall measurement system with 0.55 T magnets. Drastically different behavior is observed for the two samples, emphasizing the fundamentally different conduction mechanisms.

The commercial ITO thin film shows a positive temperature coefficient of resistance (TCR) and is consistent with metallic-like conduction described by the Bloch-Grüneisen equation, which is shown as the best-fit line in Fig. 9. On the other hand, a negative TCR was observed for the nanocrystal film. In this case, the resistance follows an exponential decay characteristic of a variable range-hopping mechanism,[30,31] seen in the figure as the best-fit line. Such behavior indicates significant potential barriers between nanocrystals, consistent with the use of the MG approximation for this nanocrystal film. However, an in-depth analysis of the electrical transport under DC fields requires more careful and complex measurements and modeling, so the fit lines in Fig. 9 are not quantitative.

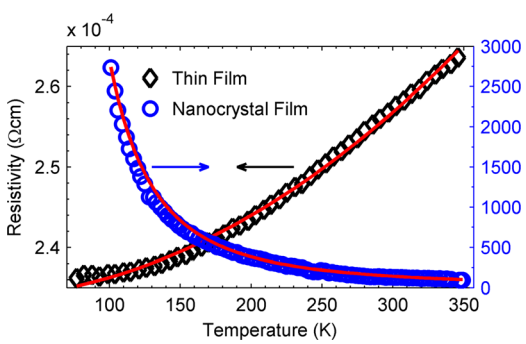

FIG. 9. Temperature-dependent resistivity measurements on the ITO thin film and nanocrystal film. The lines show the fits of the Bloch-Grüneisen and Mott variable range hopping equations, respectively.

V. CONCLUSIONS

Application of the Drude theory to *R* and *T* spectra of TCO thin films and nanocrystal films can give reliable results if care is taken. Performing only one fit to the data does not give a clear picture, and several fits using various initial guesses and parameter limits are necessary. For most TCO's, the frequency dependence of the Drude damping parameter must be accounted for and is usually attributed to ionized impurity scattering. Nevertheless, a fully empirical model for the frequency dependence allows for excellent fits to *T* and *R* with less uncertainty than a more complicated semiempirical model that attempts to represent the physics of impurity scattering.

When fitting *T* and *R* of nanocrystal films, the Maxwell-Garnett effective medium approximation can still be valid, even at relatively high volume fractions. This approximation assumes the particles are electrically isolated, which is approximately the case when the in-particle resistivity is much lower than that of the film as a whole. This results in a hopping conduction mechanism under dc fields, which is consistent with the observed negative TCR for the nanocrystal film. For the best results for thin films and nanocrystal films, both *T* and *R* should be accounted for. On the other hand, if only *T* measurements are available, the extracted optical and electrical properties are in good agreement with those found when *R* is also taken into account, although the uncertainties are about 3 times as large. Whether or not *R* is taken into account, the Drude parameters and complex refractive index extracted with the relatively fast *T* measurements are in good agreement with those found by SE.

ACKNOWLEDGMENTS

The authors acknowledge R. Buonsanti, A. Llordes, E. Runnerstrom, T.J. Richardson, A. Anders, and K.M. Yu for supporting this work. Research was supported by the LDRD Program of Lawrence Berkeley National Laboratory [Dr. Mendelsberg] and by an Office of Basic Energy Sciences Early Career Research Program grant [Dr. Milliron, G. Garcia] under U.S. Department of Energy Contract No. DE-AC02-05CH11231. Portions of this work were performed as a User project at the LBNL Molecular Foundry, which is supported by the Office of Science, Office of Basic Energy Sciences, under the same contract.

[1]J. J. Thomson, Philos. Mag. Ser. 5 **44**, 293 (1897).
[2]P. Drude, Ann. Phys. **306**, 566 (1900).
[3]R. E. Lindquist and A. W. Ewald, Phys. Rev. **135**, A191 (1964).
[4]J. Toots, H. A. Fowler, and L. Marton, Phys. Rev. **172**, 670 (1968).
[5]A. H. Kahn, Phys. Rev. **97**, 1647 (1955).

[6]H. Fujiwara and M. Kondo, Phys. Rev. B **71**, 075109 (2005).
[7]F. C. Lai, L. M. Lin, R. Q. Gai, Y. Z. Lin, and Z. G. Huang, Thin Solid Films **515**, 7387 (2007).
[8]M. Losurdo, M. Giangregorio, P. Capezzuto, G. Bruno, R. De Rosa, F. Roca, C. Summonte, J. Pla, and R. Rizzoli, J. Vac. Sci. Technol. A **20**, 37 (2002).
[9]F. Ruske, A. Pflug, V. Sittinger, B. Szyszka, D. Greiner, and B. Rech, Thin Solid Films **518**, 1289 (2009).
[10]J. Steinhauser, S. Fay, N. Oliveira, E. Vallat-Sauvain, and C. Ballif, Appl. Phys. Lett. **90**, 142107 (2007).
[11]J. Steinhauser, S. Fay, N. Oliveira, E. Vallat-Sauvain, D. Zimin, U. Kroll, and C. Ballif, Phys. Status Solidi A **205**, 1983 (2008).
[12]M. Losurdo, Thin Solid Films **455**, 301 (2004).
[13]J. Y. Kim, C. Lee, S. Bae, K. S. Kim, B. H. Hong, and E. J. Choi, Appl. Phys. Lett. **98**, 201907 (2011).
[14]I. Hamberg and C. G. Granqvist, J. Appl. Phys. **60**, R123 (1986).
[15]D. Mergel and Z. Qiao, J. Phys. D **35**, 794 (2002).
[16]J. M. Bennett and M. J. Booty, Appl. Opt. **5**, 41 (1966).
[17]G. Garcia, R. Buonsanti, E. L. Runnerstrom, R. J. Mendelsberg, A. Llordes, A. Anders, T. J. Richardson, and D. J. Milliron, Nano Lett. **11**, 4415 (2011).
[18]E. Gerlach, J. Phys. C **19**, 4585 (1986).
[19]J. Ederth, P. Heszler, A. Hultaker, G. A. Niklasson, and C. G. Granqvist, Thin Solid Films **445**, 199 (2003).
[20]S. K. O'Leary, S. R. Johnson, and P. K. Lim, J. Appl. Phys. **82**, 3334 (1997).
[21]A. Solieman and M. A. Aegerter, Thin Solid Films **502**, 205 (2006).
[22]T. S. Sathiaraj, Microelectron. J. **39**, 1444 (2008).
[23]B. E. Sernelius, K.-F. Berggren, Z.-C. Jin, I. Hamberg, and C. G. Granqvist, Phys. Rev. B **37**, 10244 (1988).
[24]S. A. Knickerbocker and A. K. Kulkarni, J. Vac. Sci. Technol. A **14**, 757 (1996).
[25]D. A. G. Bruggeman, Ann. Phys. **416**, 636 (1935).
[26]J. C. Maxwell-Garnett, Philos. Trans. R. Soc. London **205**, 237 (1905).
[27]W. Rechberger, A. Hohenau, A. Leitner, J. Krenn, B. Lamprecht, and F. Aussenegg, Opt. Commun. **220**, 137 (2003).
[28]A. Pflug, V. Sittinger, F. Ruske, B. Szyszka, and G. Dittmar, Thin Solid Films **455–456**, 201 (2004).
[29]T. Yamada, H. Makino, N. Yamamoto, and T. Yamamoto, J. Appl. Phys. **107**, 123534 (2010).
[30]A. J. Houtepen, D. Kockmann, and D. Vanmaekelbergh, Nano Lett. **8**, 3516 (2008).
[31]D. Yu, C. J. Wang, B. L. Wehrenberg, and P. Guyot-Sionnest, Phys. Rev. Lett. **92**, 216802 (2004).